

# Flux qubit-based detector of microwave photons

O. A. Ilinskaya,<sup>1,2,\*</sup> A. I. Ryzhov,<sup>1</sup> and S. N. Shevchenko<sup>1</sup>

<sup>1</sup>*B. Verkin Institute for Low Temperature Physics and Engineering, Kharkiv 61103, Ukraine*

<sup>2</sup>*G. V. Kurdyumov Institute for Metal Physics, Kyiv 03142, Ukraine*

(Dated: February 13, 2024)

A theory of detection of microwave photons with a flux qubit-based detector is presented. We consider semiclassical approximation with the electromagnetic field being in a coherent state. Flux qubit is considered as a multilevel quantum system (qudit). By solving the Lindblad equation, we describe the time evolution of occupations of the qudit's levels for readout and reset stages of detection. When considering the reset stage, the time evolution is described by multiple avoided-level crossings, thus providing a multilevel Landau-Zener-Stückelberg-Majorana (LZSM) problem. In addition to numerical calculations, we present an approximate analytical solution for the description of the reset stage dynamics based on the adiabatic-impulse approximation and rate equation approach. Our theory may be useful for the theoretical description of driven-dissipative dynamics of qudits, including applications such as single-photon detection.

## I. INTRODUCTION

Detection of microwave photons is used in various fields of physics, for example, for measuring superconducting qubits [1, 2], making two remote superconducting qubits entangled [3], imaging with a small number of photons [4], and searching dark matter axions [5]. Different studies suggest different solutions for overcoming the difficulties in detecting photons of the microwave range which are because of small energies of these photons, and there is still no prevailing technology. Some of detectors of microwave photons are based on photon-assisted tunneling in semiconducting double quantum dot circuits (see Ref. [6] for a review). Another direction of research uses superconducting circuits with Josephson junctions, which are nonlinear inductors and allow making superconducting qubits [7]. Usual single-photon detectors are destructive in the sense that a photon is absorbed making a transition of the qubit from the ground state to the excited one. This transition induces a “click” of the detector. In addition, quantum non-demolition detection of microwave photons was reported [8, 9].

Diverse types of superconducting qubits are used for detection of microwave photons — phase qubits [1, 10], flux qubits [11], transmons [8, 9]. A phase qubit is characterized by a “washboard” potential and a “click” means that a voltage is measured which is due to tunneling from the excited state of the qubit to the continuum. Tunneling from the ground state of the qubit through the barrier is also possible but the tunneling rate for this process is usually two-three orders of magnitude less than that of the excited state [10]. However, this tunneling should be also taken into account and is responsible for dark count rate (when a “click” happens without any photon). A phase qubit used in the detection scheme is called a Josephson photomultiplier [12] (see also Ref. [13]). Optimal characteristics for a phase qubit used in quantum

computing and in photodetection are different. While quantum computers need long decoherence times to operate, for photodetection a dephasing time should be sufficiently small as was argued in Ref. [12].

For a phase qubit, “working” levels are localized in one well. On the contrary, for a flux qubit these two levels belong to different potential wells (i.e., they are characterized by opposite directions of a magnetic flux, or, which is the same, by opposite direction of supercurrent flowing in the loop). Therefore, a photon arrival changes the direction of the magnetic flux, and that is measured. A flux qubit-based single-photon detector was studied both theoretically [14] and experimentally [11]. In these papers, the dressed states of a superconducting qubit represented an artificial  $\Lambda$ -type three-level system. The signal pulse was in a weak coherent state with mean photon number of order 0.1. In the experiment, the signal-pulse shape was a Gaussian function (however, the authors theoretically confirm the possibility to detect signals with rectangular and exponentially-decaying shapes). The parameters which correspond to near-perfect absorption condition were found. At these values of parameters, the reflection of the input signal is reduced.

In this paper, we study a flux qubit-based detector of microwave photons in a semiclassical approximation, which means that the input signal is in a coherent state. Unlike Ref. 14, we consider the flux qubit as a multilevel system. We note that some experimental studies of a flux qubit-based photon detector of this kind were presented in Refs. [15, 16] and the scheme of weak continuous measurement for readout of the flux qubit states was proposed [17]. Using numerical calculations, we plot the dynamics of qubit's populations for readout and reset stages of detection.

The paper is organized as follows. In Section II we write down the stationary Hamiltonian of a flux qubit and obtain stationary energy levels and eigenfunctions numerically. In Section III we discuss the principle of operation of the detector. Section IV is devoted to the calculation of the dynamics of the occupations of the lev-

\* ilinskaya@ilt.kharkov.ua

els of the multilevel system for readout and reset stages. We conclude in Section V. Appendix A contains the approximate analytical description of the reset stage dynamics.

## II. SUPERCONDUCTING FLUX QUBIT: ELECTRIC CIRCUIT, LAGRANGIAN, STATIONARY HAMILTONIAN

A superconducting flux qubit can be described by the following electric circuit (see Fig. 1(a)): a loop, which contains a Josephson junction and an inductance  $L$  and is pierced by an external magnetic flux  $\Phi_e$ . The full magnetic flux  $\Phi$  in the loop and  $\Phi_e$  are related by the transcendental equation

$$\Phi = \Phi_e - LI_c \sin\left(2\pi \frac{\Phi}{\Phi_0}\right), \quad (1)$$

which is due to the existence of a shielding current and holds for radio-frequency SQUID [18]; here  $I_c$  stands for the critical current,  $\Phi_0 = \pi\hbar/e$  is the magnetic flux quantum. The energy associated with the capacitance  $C$ ,  $C\dot{\Phi}^2/2$ , can be considered as a kinetic energy. There are two potential energy terms, i.e.  $(\Phi - \Phi_e)^2/2L$  associated with the inductance and the Josephson junction energy  $E_J[1 - \cos(2\pi\Phi/\Phi_0)]$ , with  $E_J = \Phi_0 I_c/2\pi$ . Then the Lagrangian can be written as

$$\mathcal{L} = \frac{C\dot{\Phi}^2}{2} - \frac{(\Phi - \Phi_e)^2}{2L} - E_J \left[1 - \cos\left(2\pi \frac{\Phi}{\Phi_0}\right)\right]. \quad (2)$$

The variable canonically conjugated to the flux  $\Phi$  is defined as  $Q = \partial\mathcal{L}/\partial\dot{\Phi} = C\dot{\Phi}$ . Treating magnetic flux  $\Phi$  and charge  $Q$  quantum-mechanically, the charge operator can be expressed as  $Q = -i\hbar\partial/\partial\Phi$ .

Omitting the constant term, the (stationary) Hamiltonian can be written as [19]

$$H(\Phi, Q) = \frac{Q^2}{2C} + U(\Phi, \Phi_e), \quad (3)$$

where the potential energy is given by

$$U(\Phi, \Phi_e) = -E_J \cos\left(2\pi \frac{\Phi}{\Phi_0}\right) + \frac{(\Phi - \Phi_e)^2}{2L}. \quad (4)$$

The stationary Schrödinger equation with energies measured in kelvins has the form

$$\left\{-\frac{1}{2M} \frac{\partial^2}{\partial x^2} + U(x)\right\} \Psi(x) = E\Psi(x), \quad (5)$$

with the potential energy

$$U(x) = U_0 \{-\beta_L \cos(2\pi x) + 2\pi^2(x - x_e)^2\}. \quad (6)$$

Here

$$x = \Phi/\Phi_0, \quad x_e = \Phi_e/\Phi_0, \quad (7)$$

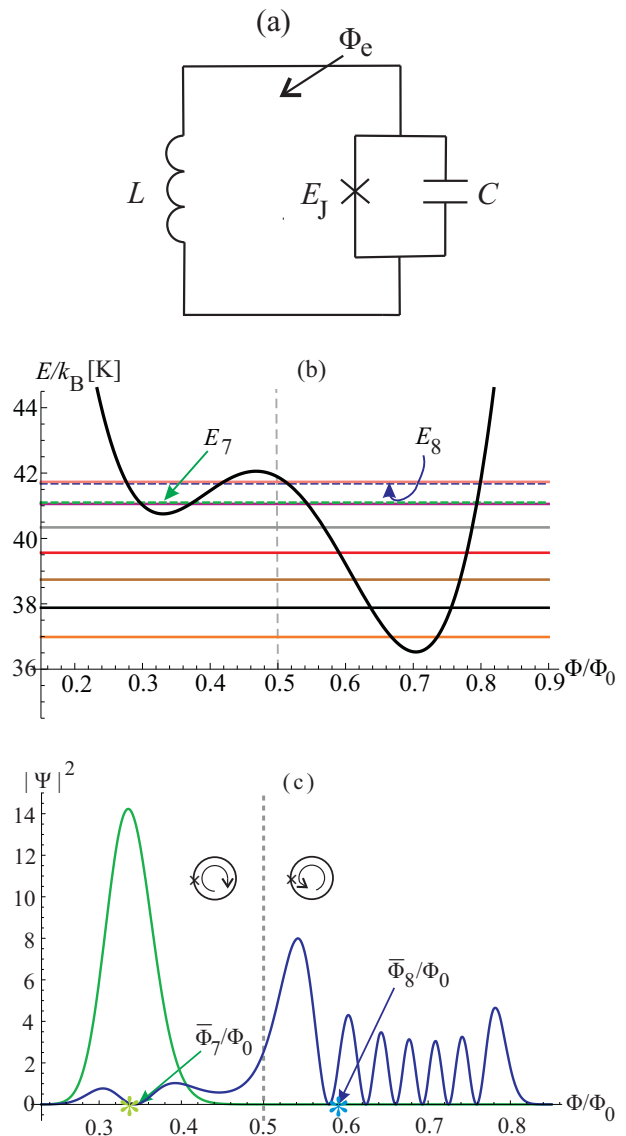


FIG. 1. (a) The electric circuit describing a superconducting flux qubit.  $E_J$  is the Josephson energy,  $L$  is the inductance,  $C$  is the capacitance,  $\Phi_e$  is the external magnetic flux. (b) The dependence of the potential energy (6) and the qubit levels' energies (in kelvins) on the magnetic flux  $\Phi$  (normalized to the magnetic flux quantum  $\Phi_0$ ). There are nine levels localized in one of the two wells. The levels, which are in resonance with incoming microwave pulse, are shown by the dashed lines (the 7th and 8th levels). Note that in the selected scale, the 6th and 7th levels are practically indistinguishable to the eye (and the same is true for the 8th and 9th levels). The proximity of the 6th and 7th (and the 8th and 9th) levels is due to splitting of levels caused by the tunneling through the barrier. (c) The square of the eigenfunction absolute value as a function of  $\Phi/\Phi_0$  for the 7th level (the green curve) and the 8th level (the blue curve). The asterisks on the x-axis denote the average values of the full magnetic flux for the two levels. Arrows inside qubit's loop show the direction of the electric current. The simulation parameters are taken close to the ones of Ref. [19]: magnetic energy  $U_0 = 32.68$  K, dimensionless inductance  $\beta_L = 1.28$ , effective mass  $M = 955$  K $^{-1}$ , external magnetic flux (in units of  $\Phi_0$ )  $x_e = 0.5087$ .

and

$$U_0 = (\Phi_0/2\pi)^2/k_B L, \quad M = k_B \Phi_0^2 C/\hbar^2, \quad (8)$$

with  $U_0$  and  $M$  being the magnetic energy and the effective mass ( $k_B$  is the Boltzmann constant);

$$\beta_L = 2\pi L I_c / \Phi_0, \quad (9)$$

is the dimensionless inductance.

The parameter  $\beta_L$  is a tunable quantity due to controllable critical current. (In practice, this tunability is realized by replacing one Josephson junction with a small loop containing two junctions.) From the analysis of Eq. (6), it follows that  $U(x)$  is a two-well potential if the double inequality holds  $1/\pi < \beta_L < 2.48$ , and we take  $\beta_L$  from this interval below. Parameters  $U_0$  and  $M$  are determined by the inductance  $L$  and capacitance  $C$  respectively, therefore, they are determined by the qubit design.

Equation (5) has a formal analogy with the Schrödinger equation for a quasiparticle with the effective mass  $M$  moving in the potential  $U(x)$ . The eigenenergies of the Hamiltonian (3) can be found numerically [19] and, for the parameters of Fig. 1 (close to those of Ref. [19]), there are nine energy levels localized in one of the wells. These levels are shown in Fig. 1(b). [We say that the level is localized in a well if its eigenfunction is localized in this well, see Fig. 1(c)]. Levels localized in different wells correspond to opposite directions of the electric current. Indeed, the external magnetic flux generates shielding current  $I_s = -I_c \sin(2\pi\Phi/\Phi_0)$  in the loop. Therefore,  $I_s < 0$  for  $\Phi/\Phi_0 < 0.5$  and  $I_s > 0$  for  $\Phi/\Phi_0 > 0.5$ .

### III. PRINCIPLE OF OPERATION OF THE PHOTON DETECTOR

Principle of operation of the flux qubit-based photon detector is shown in Fig. 2. Let the quasiparticle be on the 7th level. The incoming microwave pulse (which should be detected) is resonant with the pair of levels, namely levels 7 and 8, which are localized in the left and right wells respectively, as it can be seen from Fig. 1(b). These levels' energies are shown by the dashed lines in Fig. 1(a). The electromagnetic pulse induces the Rabi oscillations between the 7th and 8th levels. Due to dissipation, the quasiparticle falls down to the lowest level in the right well, therefore, the electric current in the loop changes its direction that corresponds to signal detection. It is necessary to distort the form of the potential (by changing the external magnetic flux  $\Phi_e$ ) in order to make the right well shallow and quasiparticle being on the 7th level so that the system is ready to register another signal.

The dependence of the levels' energies on the external magnetic flux  $\Phi_e$  is shown in Fig. 3(a). The avoided crossing, inherent to all pairs of adjacent levels, is illustrated for the 6th and 7th levels in Fig. 3(b). Fig. 3(c)

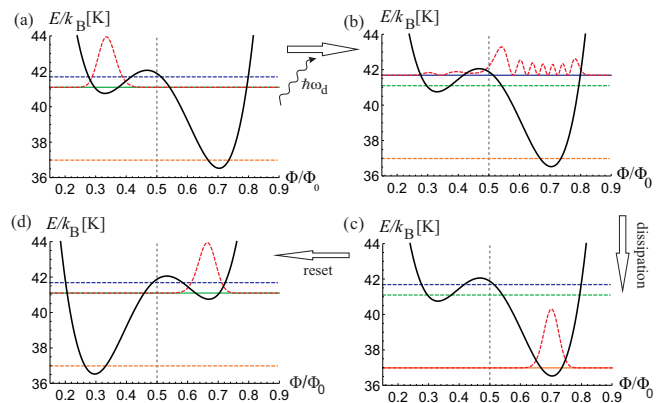


FIG. 2. The principle of operation of the photon detector. (a) The quasiparticle is on the 7th level (only the levels Nos. 1, 7, and 8 are shown, cf. Fig. 1(b)). (b) The incoming signal with the frequency  $\omega_d = (E_8 - E_7)/\hbar$  induces the Rabi oscillations between the 7th and 8th levels (the capture stage of the detection). (c) The dissipation transfers the quasiparticle to the lowest level, therefore, the change of the direction of the electric current can be measured (the readout stage of the detection). (d) Reset of the system is done by changing the external magnetic flux  $\Phi_e$  from the value 0.5087 to 0.4913 (see also Fig. 3(a)). The potential  $U(x)$  is distorted and the quasiparticle is on the 7th level again.

shows the levels' energies as functions of one of the system parameters,  $\beta_L$ .

We now estimate the speed of external magnetic flux variation which ensures a transition from the lowest level to the 7th level during the reset with sufficiently high transition probability ( $P \approx 0.99$ ). This speed  $v$  (in energy units) can be estimated from the Landau-Zener-Stückelberg-Majorana formula (see, for example, Refs. [20–22]). This formula gives the probability of diabatic transition between two energy states of a quantum system which has a time-dependent Hamiltonian with linear bias, i.e.

$$H_{\text{LZSM}} = \frac{1}{2} \begin{pmatrix} vt & \Delta \\ \Delta & -vt \end{pmatrix}. \quad (10)$$

If the system starts, in the infinite past, in the lower energy eigenstate, the probability of finding the system in the upper energy eigenstate in the infinite future, after traversing the avoided crossing region, is as follows

$$P_{\text{LZSM}} = e^{-\frac{\pi\Delta^2}{2\hbar v}}. \quad (11)$$

Now, we have a task with fixed target  $P_{\text{LZSM}}$  and several values of  $\Delta$ 's, see Fig. 3(a). Then, the minimal speed  $v$ , which is needed to achieve the target transition probability, corresponds to the largest avoided-level crossing  $\Delta_{\text{max}} \approx 3$  mK. The relation between  $v$  and the speed  $d\Phi_e/dt$  of external magnetic flux variation is the following [23]:  $d\Phi_e/dt = v/2I_p$ , where we take the persistent current  $I_p \approx \Phi/L \approx 3\mu\text{A}$ . Using this estimate and the value of  $v$  corresponding to  $P_{\text{LZSM}} = 0.99$ , we obtain

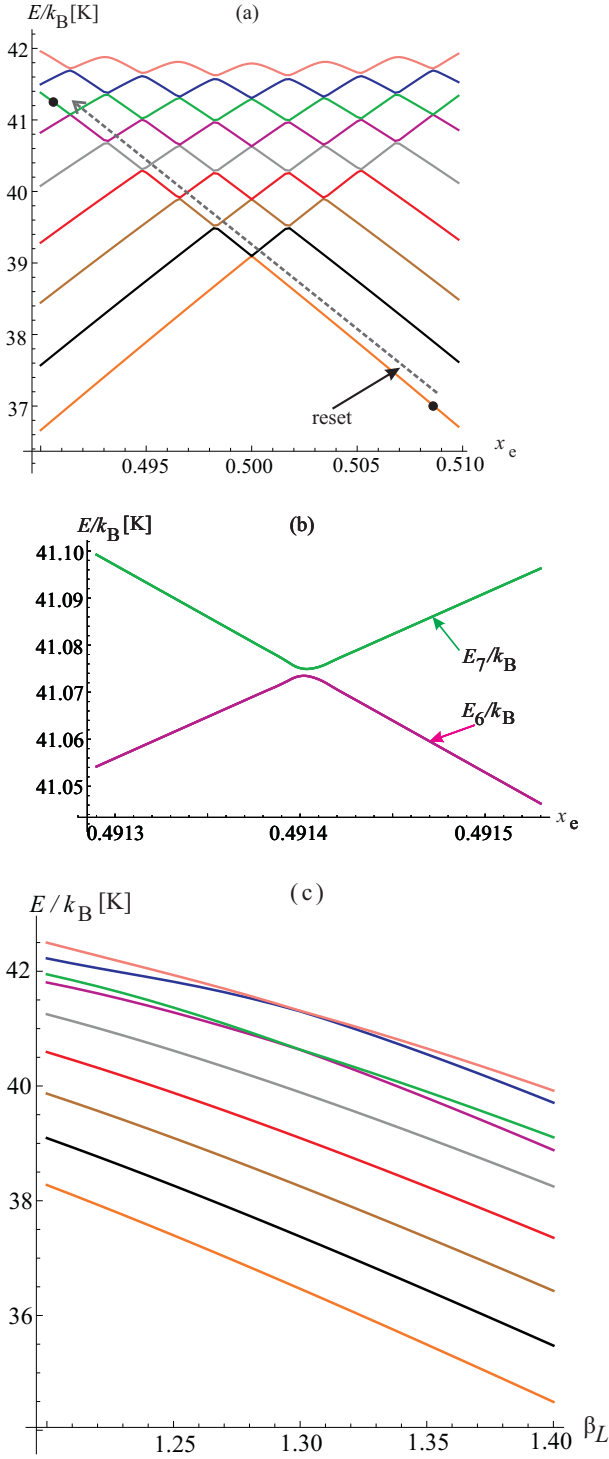


FIG. 3. (a) The qudit energy levels as a function of the external magnetic flux  $x_e$ . The energy levels exhibit quasicrossings as it is shown in panel (b) for the 6th and 7th levels. The simulation parameters are the same as in Fig. 1. (c) The dependence of the qudit energy levels on the dimensionless inductance  $\beta_L$ . The simulation parameters are  $U_0 = (41.67/\beta_L)$  K,  $M = 955$  K $^{-1}$ ,  $x_e = 0.5087$ .

$d\Phi_e/dt \approx 0.5$  nWb/s  $\approx 0.25\Phi_0/\mu$ s (note that this estimate is obtained in the absence of dissipation). This is a realistic value for rf SQUIDs. Varying  $\Phi_e$  with this speed, we need approximately  $0.1$   $\mu$ s to change  $\Phi_e$  from the initial value  $0.5087\Phi_0$  to the final value  $0.4913\Phi_0$ .

## IV. DYNAMICS

### A. Capture and readout stages

#### 1. Full Hamiltonian and semiclassical approximation

We write the Hamiltonian (3) in the basis of eigenfunctions of the qudit. Taking also into account the single-mode resonator and incoming microwave pulse, we can write down the Hamiltonian as follows [24]

$$H = \sum_{j=1}^N E_j |E_j\rangle \langle E_j| + \hbar\omega_r a^\dagger a + g(a^\dagger |E_7\rangle \langle E_8| + \text{h.c.}) + A_d f(t)(a^\dagger e^{-i\omega_d t} + \text{h.c.}). \quad (12)$$

This is the simplification of the generalized Jaynes-Cummings Hamiltonian,  $N = 9$  for the chosen parameters. By simplification, we mean that the interaction of the qudit with the electromagnetic field, described by the third term of Eq. (12), couples the field just to the 7th and 8th levels and leaves all other levels unaffected. Here  $a$  is the annihilation operator for electromagnetic field,  $E_j$  is the eigenenergy of the  $j$ th level corresponding to the eigenfunction  $|E_j\rangle$  of the qudit,  $\omega_r$  is the resonator frequency,  $g$  is the qudit-field interaction energy,  $A_d$  and  $\omega_d$  are the energy and the angular frequency of the incoming microwave pulse respectively. The signal can have almost any shape  $f(t)$ , for example, Gaussian, square, exponential [14]. Note that the Hamiltonian of a flux qubit with a single Josephson junction inductively coupled to a resonator has the form of the quantum Rabi Hamiltonian [25, 26] if we do not include into consideration the qubit's higher energy levels [27]. We note also that energy eigenstates of a flux qubit-resonator system with deep strong coupling were reported to be entangled ones [28].

We perform a unitary rotating-wave transformation,

$$U = \exp[i\omega_d t(a^\dagger a + \sum_j |E_j\rangle \langle E_j|)] \quad (13)$$

(see, for example, Ref. 29), after which the transformed Hamiltonian,  $\tilde{H} = UHU^\dagger + i\hbar\dot{U}U^\dagger$ , takes the form

$$\tilde{H} = \sum_{j=1}^N (E_j - \hbar\omega_d j) |E_j\rangle \langle E_j| + \hbar(\omega_r - \omega_d) a^\dagger a + g(a^\dagger |E_7\rangle \langle E_8| + \text{h.c.}) + A_d f(t)(a^\dagger + a). \quad (14)$$

We assume that the field is in the coherent state  $|\alpha\rangle$ , average  $\tilde{H}$  over  $|\alpha\rangle$  analogously to Ref. [30], and obtain

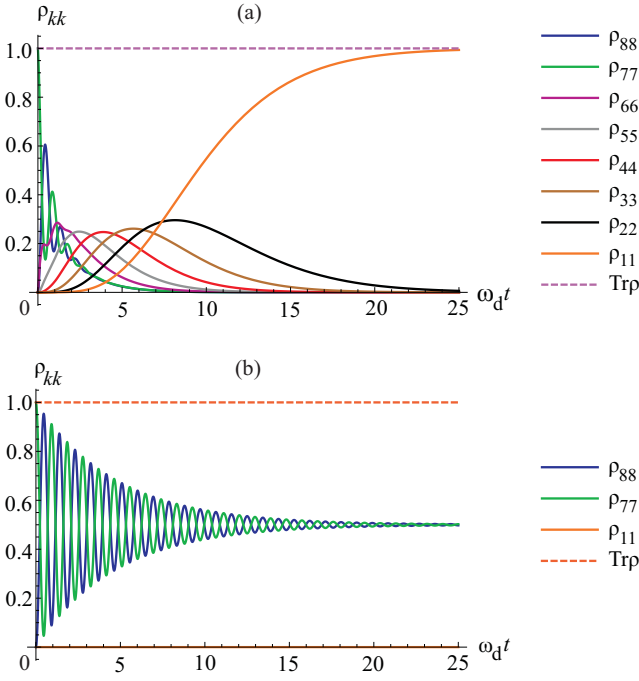


FIG. 4. Impact of relaxation and dephasing: Time dependence of the occupations of the qudit levels when (a) only energy relaxation is included into the Lindbladian [the second term in the r.h.s. of Eq. (17)] and (b) only dephasing is included into the Lindbladian [the third term in the r.h.s. of Eq. (17)]; in this figure,  $\rho_{11} = \rho_{22} = \rho_{33} = \rho_{44} = \rho_{55} = \rho_{66} = 0$ . The simulation parameters are  $U_0 = 32.68$  K,  $\beta_L = 1.28$ ,  $M = 955$  K $^{-1}$ ,  $x_e = 0.5087$ ,  $g = 2$  K,  $\alpha = 1$ , the relaxation rate is  $\gamma = 0.1$  K (approximately 2 GHz), and the dephasing rate is  $\gamma_\phi = 0.5$  K (approximately 10 GHz). The frequency of external microwave pulse is  $\hbar\omega_d = E_8 - E_7$ .

$H_c = \langle \alpha | \tilde{H} | \alpha \rangle$  in the form

$$H_c = \sum_{j=1}^N (E_j - \hbar\omega_d j) |E_j\rangle \langle E_j| + \hbar(\omega_r - \omega_d) \langle n \rangle + g(\alpha^* |E_7\rangle \langle E_8| + \text{h.c.}) + A_d f(t)(\alpha^* + \alpha), \quad (15)$$

where  $\alpha = \sqrt{\langle n \rangle}$  and  $\langle n \rangle$  is the mean photon number. Assuming for simplicity  $\alpha$  being real and omitting constants, we can rewrite Eq. (15) as follows

$$H_c = \sum_{j=1}^N (E_j - \hbar\omega_d j) |E_j\rangle \langle E_j| + g\alpha(|E_7\rangle \langle E_8| + \text{h.c.}) + 2A_d \alpha f(t). \quad (16)$$

## 2. Lindblad equation and qudit's populations dynamics

We take into account (i) energy relaxation from the 7th level to the 6th one, from the 6th level to the 5th one etc., (ii) dephasing (and we neglect dissipation in

the resonator which is assumed to be small [12]), then the Lindblad equation reads

$$\partial_t \hat{\rho} = -\frac{i}{\hbar} [H_c, \hat{\rho}] + \gamma D(b) \hat{\rho} + \gamma_\phi D(b^\dagger b) \hat{\rho}, \quad (17)$$

where  $\hat{\rho}$  is the density operator and the two last terms in the r.h.s. are the Lindblad terms [24], with  $\gamma$  and  $\gamma_\phi$  being the relaxation and dephasing rates respectively. Ladder operator  $b$  of the qudit is defined as  $b = \sum_{j=0}^{N-1} \sqrt{j+1} |j\rangle \langle j+1|$ . The upper limit in the sum is  $N-1 = 8$  (and not  $N$ ) because the “working” levels of the qudit are the 7th and 8th ones and we neglect temperature effects which could lead to the occupation of upper levels. Superoperator  $D(O)\hat{\rho}$  has the standard form [30]

$$D(O)\hat{\rho} = O\hat{\rho}O^\dagger - \frac{1}{2}O^\dagger O\hat{\rho} - \frac{1}{2}\hat{\rho}O^\dagger O. \quad (18)$$

Note that the form of the signal  $f(t)$  does not enter Eq. (17) in the semiclassical approximation.

For the capture stage (excitation) and readout stage (relaxation), the differential equation for the matrix element  $\rho_{kk'} \equiv \langle E_k | \hat{\rho} | E_{k'} \rangle$  has the form

$$\begin{aligned} \frac{d\rho_{kk'}}{dt} = & -i \left\{ \left( \frac{E_k}{\hbar} - \omega_d k \right) \rho_{kk'} - \left( \frac{E_{k'}}{\hbar} - \omega_d k' \right) \rho_{kk'} \right. \\ & + \frac{g}{\hbar} \alpha (\rho_{8k'} \delta_{k7} + \rho_{7k'} \delta_{k8} - \rho_{k7} \delta_{k'8} - \rho_{k8} \delta_{k'7}) \\ & + \gamma_{kk'} \sqrt{(k+1)(k'+1)} \rho_{k+1, k'+1} (1 - \delta_{k8})(1 - \delta_{k'8}) \\ & - \frac{1}{2} (k\gamma_k + k'\gamma_{k'}) \rho_{kk'} (1 - \delta_{k1})(1 - \delta_{k'1}) \\ & \left. + \gamma_\phi \left( kk' - \frac{k^2 + (k')^2}{2} \right) \rho_{kk'} \right\}, \quad (19) \end{aligned}$$

where the third and fourth lines include energy relaxation terms and the last line – dephasing terms;  $\delta_{kk'}$  is the Kronecker symbol. We assume for simplicity  $\gamma_{kk'} \sqrt{(k+1)(k'+1)} = k\gamma_k = k'\gamma_{k'} = \gamma$ . The system of equations (19) for  $k, k' = 1, 2, \dots, 8$  is solved numerically.

Temporal evolution of the diagonal matrix elements  $\rho_{kk}$  with only relaxation taken into account is shown in Fig. 4(a). For  $t \rightarrow \infty$ , the occupation of the lowest level tends to unity while occupations of all other levels vanish. There are damped Rabi oscillations between levels 7 and 8. An increase of  $g$  (or  $\alpha$ ) leads to the growth of the frequency of these oscillations and vice versa. (This statement is not illustrated here.) Including dephasing leads to additional dissipation of the oscillations of the “working” levels; to demonstrate this, in Fig. 4(b) we present the dissipative dynamics, neglecting relaxation,  $\gamma = 0$ .

## B. Reset stage

In order to obtain time evolution of the occupations of the qudit's energy levels during the reset stage, it is nec-

essary to solve the Lindblad equation (17) with  $H_c$  from Eq. (16) replaced by the time-dependent Hamiltonian

$$H_r(t) = \sum_{j=1}^N E_j(t) |E_j(t)\rangle \langle E_j(t)|. \quad (20)$$

Here the time dependence is due to variation of the external magnetic flux,

$$\Phi_e = \Phi_{e0} - v_e t, \quad (21)$$

with  $v_e = d\Phi_e/dt$ , and  $|E_j(t)\rangle$  is the eigenfunction corresponding to the  $j$ th adiabatic energy level  $E_j(t)$ . We denote via  $\hat{A}(t)$  the transfer matrix from the eigenenergy basis, with  $t = 0$ , to the adiabatic basis, then  $A_{kk'}(t) = \langle E_{k'}^{(0)} | E_k(t) \rangle$ , where  $|E_{k'}^{(0)}\rangle = |E_{k'}(t=0)\rangle$ . Note that the problem of reset is, in fact, the ‘‘equal-slope’’ multi-level Landau-Zener-Stückelberg-Majorana problem (see Ref. [22] for a review).

Taking into account that

$$\begin{aligned} \langle E_k(t) | \frac{d\hat{\rho}}{dt} | E_{k'}(t) \rangle &= \frac{d}{dt} \langle E_k(t) | \hat{\rho} | E_{k'}(t) \rangle \\ &- \frac{d\langle E_k(t) |}{dt} \hat{\rho} | E_{k'}(t) \rangle - \langle E_k(t) | \hat{\rho} \frac{d|E_{k'}(t)\rangle}{dt} \end{aligned} \quad (22)$$

and neglecting dephasing ( $\gamma_\phi = 0$ ), we obtain the differential equation for the matrix element  $\rho_{kk'} \equiv \langle E_k(t) | \hat{\rho} | E_{k'}(t) \rangle$  for the reset stage in the form

$$\begin{aligned} \frac{d\rho_{kk'}}{dt} &= \left( \hat{B}^*(t) \hat{\rho} \right)_{kk'} + \left( \hat{B}(t) \hat{\rho}^* \right)_{k'k} \\ &- \frac{i}{\hbar} \left( E_k(t) - E_{k'}(t) \right) \rho_{kk'} \\ &+ \gamma_{kk'} \sqrt{(k+1)(k'+1)} \rho_{k+1, k'+1} (1 - \delta_{k7})(1 - \delta_{k'7}) \\ &- \frac{1}{2} (k\gamma_k + k'\gamma_{k'}) \rho_{kk'} (1 - \delta_{k1})(1 - \delta_{k'1}), \end{aligned} \quad (23)$$

where  $k, k' = 1, 2, \dots, 7$  and

$$\hat{B}(t) = \frac{d\hat{A}(t)}{dt} \hat{A}^{-1}(t). \quad (24)$$

We plot the dependence of the occupations of the qudit levels on the external magnetic flux  $x_e$  for the reset stage in Fig. 5(a). Note that we take the speed  $v_e$  of the external magnetic flux variation much larger than the minimal necessary value which we obtained as an estimate in Section III. There is a technical reason for it as the larger the speed, the less the time of numerical calculations. Due to large value of  $v_e$ , the characteristic widths of the transitions are small and vary from  $10^{-9}$  (in units of magnetic flux quantum) for the first transition to  $10^{-5}$  for the last transition. The probability  $P_r$  to return to level 7 from level 1 can be estimated as a product of probabilities of transitions between adjacent levels multiplied by  $\exp(-\gamma\delta t)$ , where  $\delta t = \delta x_e/v_e$  is the time of transition, with  $\delta x_e$  being the magnitude of change of

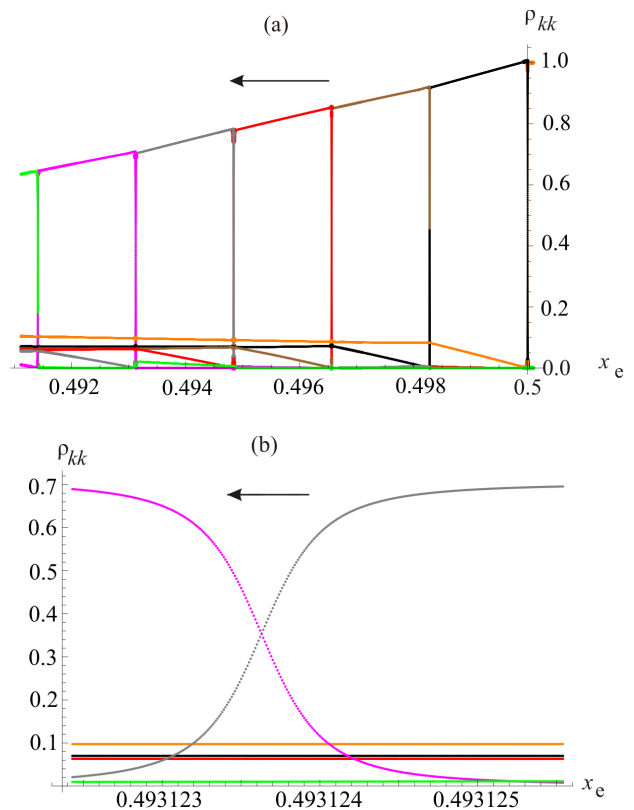


FIG. 5. (a) The dependence of the occupations of the qudit levels on the dimensionless external magnetic flux  $x_e$  that describes the reset stage of the detection. The change of  $x_e$  is towards lower values. The orange curve corresponds to level 1, the black curve – to level 2, the brown curve – to level 3, the red curve – to level 4, the gray curve – to level 5, the magenta curve – to level 6, the green curve – to level 7. The simulation parameters are  $U_0 = 32.68$  K,  $\beta_L = 1.28$ ,  $M = 955$  K $^{-1}$ ,  $\tilde{v}_e (= v_e/\Phi_0) = 0.454$  GHz,  $\gamma = 22.7$  GHz. We take the initial value of external magnetic flux in Eq. (21) as follows:  $\Phi_{e0} = 0.5001\Phi_0$  instead of  $0.5087\Phi_0$  (compare Fig. 1) because the dynamics for the values of external magnetic flux larger than  $0.5\Phi_0$  is trivial (there are no any transitions). (b) The same dependence as in (a) near the point of quasicrossing of levels 5 (gray) and 6 (magenta). The characteristic width of this transition in units of magnetic flux is about  $10^{-6}\Phi_0$ .

$x_e$  which can be determined from Fig. 5(a). This estimate gives  $P_r \approx 0.64$  which is in good agreement with numerical result of Fig. 5(a). Fig. 5(b) shows a part of this graph corresponding to LZSM transition from level 5 to level 6.

The dependence of the occupations  $\rho_{kk}$  of the qudit levels on  $x_e$  can be approximately calculated: (i) by the adiabatic-impulse model in the absence of dissipation (see Appendix A 1) and (ii) by combination of the adiabatic-impulse model and the rate equation approach in the presence of dissipation (see Appendix A 2). The approximate analytical method presented in Appendix A 2 gives  $x_e$ -dependence of  $\rho_{kk}$  which, for chosen parameters, is in a sufficiently good agreement with the results obtained

by numerically solving the system of equations (23) and shown in Fig. 5(a), despite the fact that this approximation does not take into account the specificity of the problem, e.g., the form of the potential  $U(x)$  in Eq. (6).

## V. CONCLUSIONS

In summary, we have considered photon detector based on the flux qubit as a multilevel system. Treating electromagnetic field semiclassically and numerically solving the Lindblad equation, we have calculated the dynamics of the occupations of the levels for the readout stage of the detection and obtained that the form of signal does not enter the results for approximations used. We can conclude from the plot showing the dynamics for the readout stage that an input signal leads to a change of the magnetic flux direction. Also, we have investigated the reset stage of the detection. We have calculated the occupations of the levels as a function of the external magnetic flux and compared numerically obtained transition probability with a simple analytical estimate.

## ACKNOWLEDGEMENTS

We would like to thank O. M. Bahrova, P. Febvre, O. Yu. Kitsenko, V. Yu. Lyakhno, and O. G. Turutanov for fruitful discussions and S. Ashhab for critically reading this manuscript. We acknowledge the support from the IEEE program “Magnetism for Ukraine 2023”. O.A.I. was supported by NATO Science for Peace and Security Program (Project G5796) and by Grant of the NAS of Ukraine for young scientists “Mesoscopic systems for quantum interferometry and detection of single photons” (Grant Number 0123U103073).

### Appendix A: Adiabatic-impulse model and rate equation approach for a multilevel quantum system

#### 1. Simplified adiabatic-impulse model without relaxation

In the absence of relaxation, the dynamics of the reset stage of the detection, illustrated in Fig. 5(a), can also be obtained by an approximate analytical method, the adiabatic-impulse model (see Refs. [22, 31]).

In this model, the whole dynamics is considered as a series of periods of the adiabatic evolution when the occupations of the energy levels are constant and the diabatic transitions, occurring at the passages of the adiabatic energy-level quasicrossings with the change of the level occupations. Generally, in the adiabatic-impulse model, we calculate the matrices of these diabatic transitions and matrices of the adiabatic evolution, and the matrix of the evolution for the whole dynamics is calculated as a multiplication of them.

We consider a particular case, namely, (i) energy levels are as in Fig. 3(a), (ii) the external magnetic flux  $\Phi_e$  linearly depends on time (see Eq. (21)), (iii) only the lowest energy level is populated in the initial state. In this case, there is a passage of quasicrossings one by one (see the dashed arrow in Fig. 3(a)) with no interference and the occupations of the adiabatic energy levels during the reset can also be found using the following simple consideration. The occupations of the energy levels are constant during the dynamics far from the quasicrossings. During the passage of the  $n$ -th quasicrossing on the path shown by the dashed arrow in Fig. 3(a) with the minimal splitting  $\Delta_n$  between the adiabatic energy levels  $E_n$  and  $E_{n+1}$ , the probability of tunneling to the upper energy level  $E_{n+1}$  equals

$$\mathcal{P}_n = \exp[-\pi\Delta_n^2/2\hbar v] \quad (\text{A1})$$

[see Eq. (11)] and the probability of remaining on the same energy level  $E_n$  equals  $1 - \mathcal{P}_n$ . This allows to find the occupations of all energy levels for all adiabatic evolution intervals during the reset process. In particular, for the final state the occupation probabilities are given by (see also Ref. [32]):

$$\begin{aligned} \rho_{11} &= 1 - \mathcal{P}_1, \\ \rho_{22} &= \mathcal{P}_1(1 - \mathcal{P}_2), \\ \rho_{kk} &= \prod_{n=1}^{k-1} \mathcal{P}_n(1 - \mathcal{P}_k), \quad k = 3, \dots, 6 \\ \rho_{77} &= \prod_{n=1}^6 \mathcal{P}_n. \end{aligned} \quad (\text{A2})$$

#### 2. Rate equation approach

In the presence of relaxation, the considered simplified adiabatic-impulse model can be combined with the rate equation approach (see Ref. [33]).

For each interval of the adiabatic evolution, we can write the system of rate equations

$$\begin{aligned} \frac{d\rho_{11}}{dt} &= \gamma_2\rho_{22}, \\ \frac{d\rho_{nn}}{dt} &= \gamma_{n+1}\rho_{n+1,n+1} - \gamma_n\rho_{nn}, \quad n = 2, \dots, 6, \\ \frac{d\rho_{77}}{dt} &= -\gamma_7\rho_{77}, \end{aligned} \quad (\text{A3})$$

where  $\gamma_n = \gamma$  is the energy relaxation rate from  $E_n$  to  $E_{n-1}$  energy level. The initial condition at  $t_0 = 0$  which corresponds to  $\Phi_e = \Phi_{e0}$  (see Eq. (21) and caption to Fig. 5(a)) is  $\rho_{11}(0) = 1$ ,  $\rho_{nn}(0) = 0$  for  $n = 2, \dots, 7$ . The initial condition at the point  $t_{12}$ , which corresponds to the first quasicrossing point  $\Phi_e = \Phi_0/2$ , is obtained taking into account the solution of the system (A3) at the point  $t_{12} - 0$ , i.e.  $\rho_{11}(t_{12} - 0) = 1$ ,  $\rho_{nn}(t_{12} - 0) = 0$  ( $n = 2, \dots, 7$ ), and the fact that there is a transition

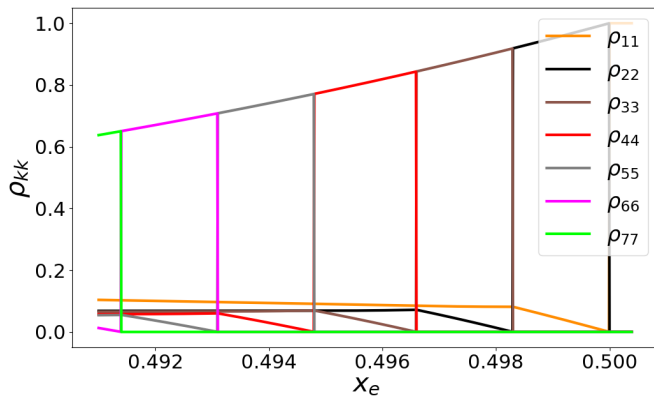


FIG. 6. The dependence of the occupation probabilities  $\rho_{kk}$  of the qudit levels on the dimensionless external magnetic flux  $x_e$  during the reset stage of the detection obtained by using the adiabatic-impulse model and rate equation approach. The energy splittings obtained by numerically solving the Schrödinger equation (5) are as follows:  $\Delta_1 = 3 \times 10^{-8}$  K,  $\Delta_2 = 7 \times 10^{-5}$  K,  $\Delta_3 = 4 \times 10^{-4}$  K,  $\Delta_4 = 0.001$  K,  $\Delta_5 = 0.002$  K,  $\Delta_6 = 0.003$  K. All parameters are the same as in Fig. 5(a).

from the level  $E_1$  to the level  $E_2$  at the point  $t_{12}$  with the probability  $\mathcal{P}_1$  (see Eq. (A1)). Therefore, the initial

condition at the point  $t_{12}$  is as follows  $\rho_{11}(t_{12}) = 1 - \mathcal{P}_1$ ,  $\rho_{22}(t_{12}) = \mathcal{P}_1$ ,  $\rho_{nn}(t_{12}) = 0$  ( $n = 3, \dots, 7$ ). The solution of the system (A3) in the interval  $(t_{12} + 0, t_{23} - 0)$  reads

$$\begin{aligned} \rho_{11}(t) &= 1 - \mathcal{P}_1 e^{-\gamma(t-t_{12})}, \\ \rho_{22}(t) &= \mathcal{P}_1 e^{-\gamma(t-t_{12})}, \\ \rho_{nn}(t) &\equiv 0, \quad n = 3, \dots, 7, \end{aligned} \quad (\text{A4})$$

where  $t_{23}$  corresponds to the point of quasicrossing between 2nd and 3rd levels. The system of equations (A3) is solved on all subsequent intervals analogously.

For the reset, the dependence of the levels occupations on the dimensionless external magnetic flux obtained by the approximate rate equation approach is illustrated in Fig. 6, and it is in a sufficiently good agreement with the dependence in Fig. 5(a) obtained by solving the system of equations (23) for the matrix elements of the density operator. The rate equation approach gives the final occupation of the 7th energy level as follows

$$\rho_{77} = \prod_{n=1}^6 \mathcal{P}_n e^{-\gamma(t-t_{12})}, \quad (\text{A5})$$

where  $t_{67} < t < t_{78}$ ,  $t_{78}$  corresponds to the point of quasicrossing between 7th and 8th levels.

- 
- [1] A. Opremcak, I. V. Pechenezhskiy, C. Howington, B. G. Christensen, M. A. Beck, E. Leonard Jr., J. Suttle, C. Wilen, K. N. Nesterov, G. J. Ribeill, T. Thorbeck, F. Schlenker, M. G. Vavilov, B. L. T. Plourde, R. McDermott, Measurement of a superconducting qubit with a microwave photon counter, *Science* **361**, 1239 (2018).
- [2] A. Opremcak, C. H. Liu, C. Wilen, K. Okubo, B. G. Christensen, D. Sank, T. C. White, A. Vainsencher, M. Guistina, A. Megrant, B. Burkett, B. L. T. Plourde, and R. McDermott, High-fidelity measurement of a superconducting qubit using an on-chip microwave photon counter, *Phys. Rev. X* **11**, 011027 (2021).
- [3] P. Campagne-Ibarcq, E. Zalus-Geller, A. Narla, S. Shankar, P. Reinhold, L. Burkhardt, C. Axline, W. Pfaff, L. Frunzio, R. J. Schoelkopf, and M. H. Devoret, Deterministic remote entanglement of superconducting circuits through microwave two-photon transitions, *Phys. Rev. Lett.* **120**, 200501 (2018).
- [4] P. A. Morris, R. S. Aspden, J. E. C. Bell, R. W. Boyd, and M. J. Padgett, Imaging with a small number of photons, *Nat. Commun.* **6**, 5913 (2015).
- [5] I. G. Irastorza and J. Redondo, New experimental approaches in the search for axion-like particles, *Prog. Part. Nucl. Phys.* **102**, 89 (2018).
- [6] A. Ghirri, S. Cornia, and M. Affronte, Microwave photon detectors based on semiconducting double quantum dots, *Sensors* **20**, 4010 (2020).
- [7] X. Gu, A. F. Kockum, A. Miranowicz, Y.-x. Liu, and F. Nori, Microwave photonics with superconducting quantum circuits, *Phys. Rep.* **718-719**, 1 (2017).
- [8] S. Kono, K. Koshino, Y. Tabuchi, A. Noguchi, and Y. Nakamura, Quantum non-demolition detection of an itinerant microwave photon, *Nat. Phys.* **14**, 546 (2018).
- [9] J.-C. Besse, S. Gasparinetti, M. C. Collodo, T. Walter, P. Kurpiers, M. Pechal, C. Eichler, and A. Wallraff, Single-shot quantum nondemolition detection of individual itinerant microwave photons, *Phys. Rev. X* **8**, 021003 (2018).
- [10] Y.-F. Chen, D. Hover, S. Sendelbach, L. Maurer, S. T. Merkel, E. J. Pritchett, F. K. Wilhelm, and R. McDermott, Microwave photon counter based on Josephson junctions, *Phys. Rev. Lett.* **107**, 217401 (2011).
- [11] K. Inomata, Z. Lin, K. Koshino, W. D. Oliver, J.-S. Tsai, T. Yamamoto, and Y. Nakamura, Single microwave-photon detection using an artificial  $\Lambda$ -type three-level system, *Nat. Commun.* **7**, 12303 (2016).
- [12] L. C. G. Govia, E. J. Pritchett, S. T. Merkel, D. Pineau, F. K. Wilhelm, Theory of Josephson photomultipliers: Optimal working conditions and back action, *Phys. Rev. A* **86**, 032311 (2012).
- [13] E. V. Stolyarov, O. V. Kliushnichenko, V. S. Kovtoniuk, and A. A. Semenov, Photon-number resolution with microwave Josephson photomultipliers, *Phys. Rev. A* **108**, 063710 (2023).
- [14] K. Koshino, K. Inomata, Z. Lin, Y. Nakamura, and T. Yamamoto, Theory of microwave single-photon detection using an impedance-matched  $\Lambda$  system, *Phys. Rev. A* **91**, 043805 (2015).
- [15] A. P. Shapovalov, V. E. Shaternik, O. G. Turutanov, V. Yu. Lyakhno, V. I. Shnyrkov, On the possibility of faster detection of magnetic flux changes in a single-photon counter by RF SQUID with MoRe-Si(W)-MoRe



- junction, *Low Temp. Phys.* **45**, 776 (2019).
- [16] V. Yu. Lyakhno, O. G. Turutanov, A. P. Boichenko, A. P. Shapovalov, A. A. Kalenyuk, V. I. Shnyrkov, Hybrid shield for microwave single-photon counter based on a flux qubit, *Low Temp. Phys.* **48**, 228 (2022).
- [17] V. I. Shnyrkov, Wu Yangcao, O. G. Turutanov, V. Yu. Lyakhno, and A. A. Soroka, Scheme for flux-qubit-based microwave single-photon counter with weak continuous measurement, 2020 IEEE Ukrainian Microwave Week, p. 737.
- [18] V. V. Schmidt, *The physics of superconductors. Introduction to fundamentals and applications*, Springer (1997), p. 93.
- [19] V. I. Shnyrkov, Wu Yangcao, A. A. Soroka, O. G. Turutanov, and V. Yu. Lyakhno, Frequency-tuned microwave-photon counter based on a superconductive quantum interferometer, *Low Temp. Phys.* **44**, 213 (2018).
- [20] S. Ashhab, O. A. Ilinskaya, and S. N. Shevchenko, Nonlinear Landau-Zener-Stückelberg-Majorana problem, *Phys. Rev. A* **106**, 062613 (2022).
- [21] P. O. Kofman, S. N. Shevchenko, and F. Nori, Tuning the initial phase to control the final state of a driven qubit, *Phys. Rev. A* **109**, 022409 (2024).
- [22] O. V. Ivakhnenko, S. N. Shevchenko, and F. Nori, Nonadiabatic Landau-Zener-Stückelberg-Majorana transitions, dynamics, and interference, *Phys. Rep.* **995**, 1 (2023).
- [23] A. N. Omelyanchouk, S. N. Shevchenko, Ya. S. Greenberg, O. Astafiev, and E. Il'ichev, Quantum behavior of a flux qubit coupled to a resonator, *Low Temp. Phys.* **36**, 893 (2010).
- [24] P. Brookes, G. Tancredi, A. D. Patterson, J. Rahamim, M. Esposito, T. K. Mavrogordatos, P. J. Leek, E. Ginossar, M. H. Szymanska, Critical slowing down in circuit quantum electrodynamics, *Sci. Adv.* **7**, eabe9492 (2021).
- [25] I. I. Rabi, Space quantization in a gyrating magnetic field, *Phys. Rev.* **51**, 652 (1937).
- [26] E. T. Jaynes and F. W. Cummings, Comparison of quantum and semiclassical radiation theories with application to the beam maser, *Proc. IEEE* **51**, 89 (1963).
- [27] F. Yoshihara, S. Ashhab, T. Fuse, M. Bamba, and K. Semba, Hamiltonian of a flux-qubit-LC oscillator circuit in the deep-strong-coupling regime, *Sci. Rep.* **12**, 6764 (2022).
- [28] F. Yoshihara, T. Fuse, S. Ashhab, K. Kakuyanagi, S. Saito, and K. Semba, Superconducting qubit-oscillator circuit beyond the ultrastrong-coupling regime, *Nat. Phys.* **13**, 44 (2017).
- [29] B. Baker, A. C. Y. Li, N. Irons, N. Earnest, and J. Koch, Adaptive rotating-wave approximation for driven open quantum systems, *Phys. Rev. A* **98**, 052111 (2018).
- [30] S. N. Shevchenko, Mesoscopic physics meets quantum engineering, World Scientific (2019).
- [31] A. I. Ryzhov, O. V. Ivakhnenko, S. N. Shevchenko, M. F. Gonzalez-Zalba, Franco Nori, Alternative fast quantum logic gates using nonadiabatic Landau-Zener-Stückelberg-Majorana transitions, arXiv:2310.17932.
- [32] S. Ashhab, T. Fuse, F. Yoshihara, S. Kim, and K. Semba, Controlling qubit-oscillator systems using linear parameter sweeps, *New J. Phys.* **25**, 093011 (2023).
- [33] M. P. Liul, A. I. Ryzhov, and S. N. Shevchenko, Interferometry of multi-level systems: rate-equation approach for a charge qudit, *Eur. Phys. J. Spec. Top.* (2023).